11th Australasian Fluid Mechanics Conference
University of Tasmania, Hobart, Australia
14-18 December 1992

STRUCTURE INVESTIGATION IN A TURBULENT BOUNDARY LAYER USING ORTHOGONAL X-WIRE ARRAYS

P.-A. KROGSTAD[1], R.A. ANTONIA[2] and L.W.B. BROWNE[2]

[1]Division of Hydro & Gas Dynamics, University of Trondheim, N-7034, NORWAY

[2]Department of Mechanical Engineering, University of Newcastle, NSW 2308, AUSTRALIA

ABSTRACT

This note focuses on details of the experimental technique used to obtain simultaneous velocity measurements from two orthogonal arrays of X-wires and its potential for capturing/extracting information on various aspects of the organized motion. The experiments were carried out in a rough wall turbulent boundary layer in an attempt to obtain some insight into the 3-D nature of the large scale motion.

INTRODUCTION

Simultaneous information on all three velocity components throughout a three-dimensional flow region has been provided by direct numerical simulation (e.g. Kim et al. 1987 for a turbulent channel flow, Spalart 1988 for a turbulent boundary layer) for low Reynolds numbers and simple boundary conditions (e.g. smooth walls). From an experimental perspective, particle image velocimetry or PIV seems potentially attractive in terms of providing simultaneous information in the velocity field at multiple points in space. Nishino and Kasagi (1989) showed that statistics of the three velocity fluctuations measured by this technique in a fully developed turbulent channel flow are generally in good agreement with the DNS data of Kim et al. (1987), both data sets being at approximately the same Reynolds number.

Another experimental approach which, like the DNS and PIV, provides the opportunity of combining "computer" flow visualization with quantitative data involves using spatial arrays of X-probes, each measuring the two velocity components in the plane of the probe. Such an approach was used by Hussain and Hayakawa (1987) and Bisset et al. (1990) to examine several aspects of the large scale motion in the wake of a circular cylinder. It has also been used in a boundary layer to provide topology details of the organised motion in both the (x,y) and (x,z) planes, although not at the same time. The main limitation of this approach (vis à vis DNS and PIV) is the relatively poor spatial resolution, due to the finite separation between the X-probes. As a consequence, only aspects associated with the large scale motion can be examined. Unlike PIV, the method provides a countinuous time record and can be used at significantly higher Reynolds numbers than is at present possible with either DNS or PIV.

EXPERIMENTAL SETUP

A rough surface, consisting of a woven stainless steel mesh screen of 0.69 mm wires, was attached to one wall of the test section in an open return wind tunnel. The free stream velocity, U_e, was 20 m/s. At the measurement station, the friction velocity, u_τ, was 1.0 m/s and the boundary layer thickness, δ, was 75 mm. The Reynolds number $R_\theta = U_e\theta/\nu$ was 12800. Full details of the set-up and the flow characteristics are given in Krogstad and Browne (1991).

Sixteen slender X-wire probes were used, arranged in two mutually orthogonal arrays, each containing 8 X-wires. The X-wires in array 1 (Figure 1) were parallel to the y axis while those in array 2 were parallel to z. The X-wires of both arrays were located at the same streamwise position. The nominal separation between probes in array 1 was 4.4 mm, so that the overall distance covered by the array was 0.41 δ. This rake was mounted on a traverse which allowed it to be positioned anywhere within the layer and moved to the free stream for calibration. Array 2 was mounted on a separate traverse mechanism. The design was such that array 2 was divided into two almost identical halves. The nominal probe separation in each half of this rake was 5 mm although, to make room for array 1, the central probes

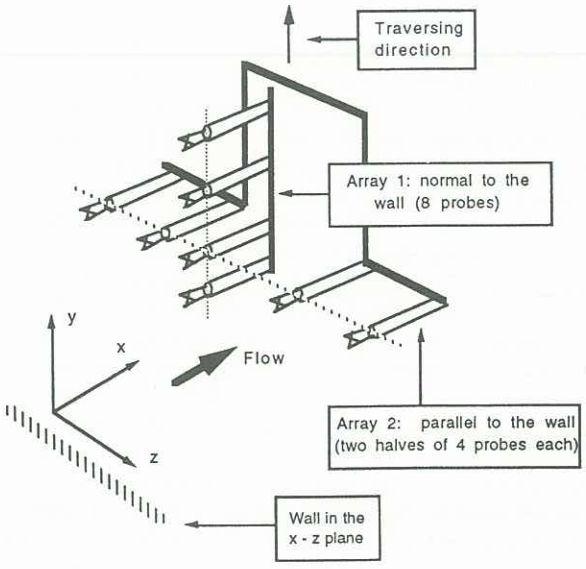

Figure 1 Sketch of the orthogonal X-wire rakes

were separated by 14 mm. The spanwise extent of array 2 was 0.59 δ.

The wires of array 1 were arranged to measure u and v (the velocities in the x and y direction) while the wires of array 2 were arranged to measure u and w (w being the velocity in the z direction). Array 1 was fixed with the first probe as close to the wall as possible. Sets of data were taken for various locations of array 2, each of which corresponding to one of the probe locations of array 1.

In order to test the effect of rake blockage, array 1 was kept at a fixed location with the first probe as close to the wall as possible. Array 2 was then traversed to the positions cooresponding to the various probes of rake 1 while the outputs of array 1 were monitored. The largest change in the mean velocity, which was less than 0.7 %, was found for the probe of array 1 closest to the wall when array 2 was located at the same height.

In-house anemometers, amplifiers and filters were used for each of the 32 hot wires. Two NEC 386 computers were used for data logging, one for each rake. The A/D systems were 16 channel, 12 bits simultaneous sampling units. Data sampling was synchronized by a common external trigger pulse provided by a signal generator and it was established that the data obtained by the two systems were simultaneous. Sampling was carried out at a frequency of 5 kHz per channel while the anemometer filters were set at 2.5 kHz. A sketch of the measurement system is shown in figure 2.

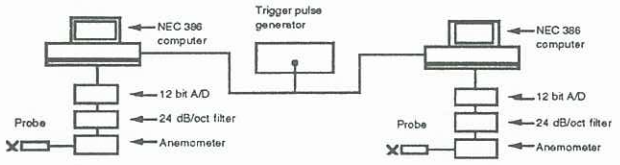

Figure 2 The experimental set-up

Yaw calibrations to determine wire effective angles were carried out external to the tunnel. Velocity calibrations were carried out, with both rakes in place, in the free stream immediately prior to collecting data.

DATA REDUCTION AND INTERPOLATION

The data from the arrays allowed the velocity vectors to be constructed in the (x,y) and (x,z) planes. To improve the sensitivity (but not the accuracy) interpolation between the experimental values was carried out using cubic splines. Following interpolation in space and time, the velocity vector pattern in the (x,y) plane was built up as follows. At each position and for each time step the velocity vector was drawn so that U = - $\overline{U}$ - u + U_r and V = v. Here $\overline{U}$ is the local mean velocity in the x direction, u and v are the fluctuating parts of the velocity and U_r is the constant velocity of an observer moving in the same direction as the flow. It was chosen to be equal to $\overline{U}$ at the intersection between the two rakes. The local mean velocity perpendicular to the wall was small enough to be neglected without loss of accuracy. The same procedure was used for the other plane. A typical set of velocity vectors obtained by the above technique is shown in figure 3. The flow is right to left. The time axis has been converted to a non-dimensional distance by means of the transformation $X^* = -tU_r/\delta$ where t is the elapsed time.

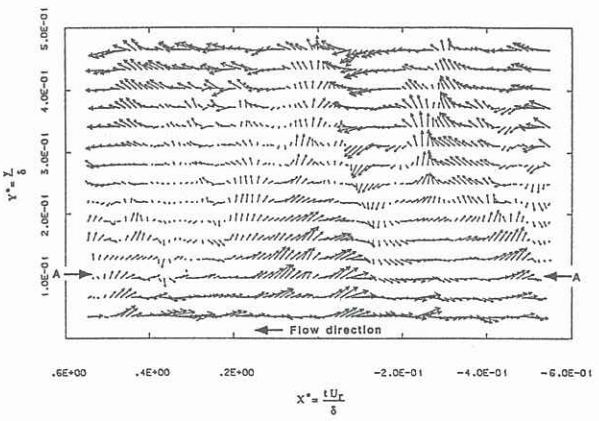

Figure 3 Instantaneous vector plots in the (x,y) plane with a single interpolation in x (time) and y.

In this case the intersection between the two arrays was located at $y/\delta = 0.11$, where $\overline{U}/U_e = 0.53$. Figure 3 shows the results obtained in the (x,y) plane using one interpolation in either direction. Figure 4 shows the set of velocity vectors in the (x,z) plane obtained simultaneously with those of figure 3. The interpolated data was equispaced in the z-direction, thus allowing the gap between the two halves of the array to be filled. The data in this region may be somewhat uncertain, but a comparison between results before and after interpolation showed that the general flow patterns have been preserved. Figures 3 and 4 intersect along the lines marked A - A .

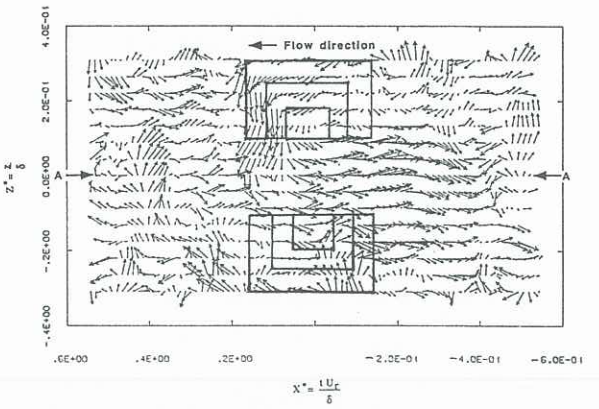

Figure 4 Instantaneous vector plots in the (x,z) plane with a single interpolation in x (time) and z.

RESULTS

The segments in figures 3 and 4 were selected arbitrarily and show about 7.5 ms out of the 20 seconds of data recorded. At $X^* \approx$ -0.4 and 0 large scale activities in the (x,y) plane may be observed which bring fluid across the entire measurement domain. Similar δ-scale motions may be observed in the (x,z) plane. Closer inspection also reveals the presence of smaller structures.

Figure 5 shows sectional streamlines for the set of data shown in figure 3 and 4 computed using the method of Bisset et al. (1990). Near $X^* \approx 0$ in the (x,y) plane a vertical displacement of fluid away from the wall may be identified as a strong ejection. It is followed by a sweep

from $Y^* \approx 0.3$ which ends at the wall. In the (x,z) plane a significant movement of fluid from the upper edge towards the center may be observed. Also a number of smaller scale structures in the two planes are seen to exist.

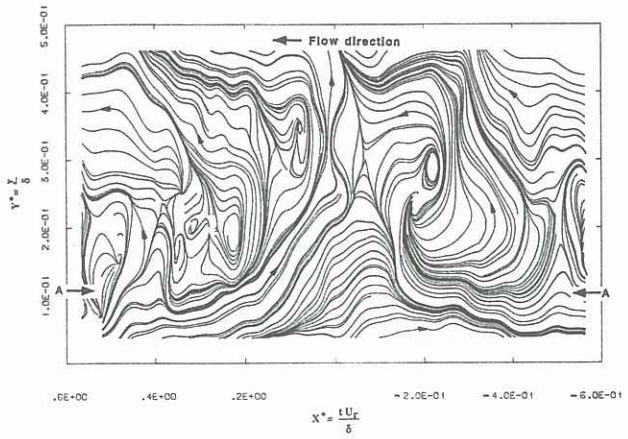

Figure 5 a. Sectional streamlines in the (x,y) plane.

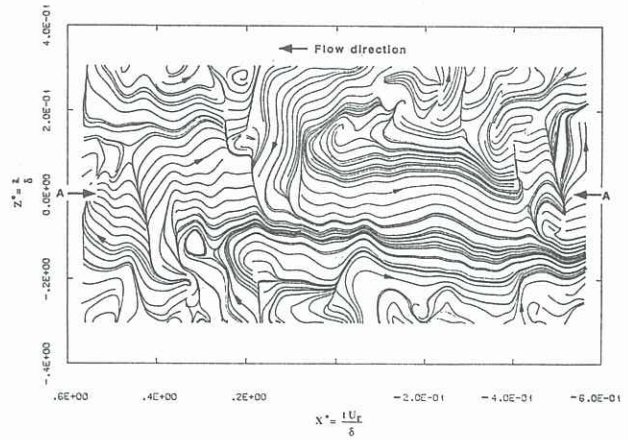

Figure 5 b. Sectional streamlines in the (x,z) plane.

Since the potential of the use of orthogonal arrays lies in detecting large structures, the data were analyzed using the Quadrant method of Lu and Wilmarth (1973), set up to detect strong events. Using the threshold $H = \mid uv \mid_n / u'v' = 4$, where n denotes the quadrant for which the detections are made, the probe located in array 1 at the intersection of the two arrays was examined for quadrant 2 and 4 events (these may possibly be identified with strong ejections and sweeps). Using these detections, the conditional averages for all probes were constructed. In this way, spatial information about the structures detected is obtained. Figure 6 shows the conditionally averaged sectional streamlines for the Q2 events based on 384 detections. $X^* = 0$ denotes the common detection point. The mean time between the ejections was found to be $\overline{T} = Tu_\tau/\delta = 0.70$ and the mean duration $\overline{\Delta T} = \Delta T u_\tau/\delta = 0.0040$. Figure 6 (a) shows that the averaged strong ejection extends from the wall to about 25 % of the layer thickness. Q2 events also show a strong correlation in the lateral plane where an almost symmetric pattern of vortical motion centered at $Z^* \approx 0.25$ may be seen (figure 6 b).

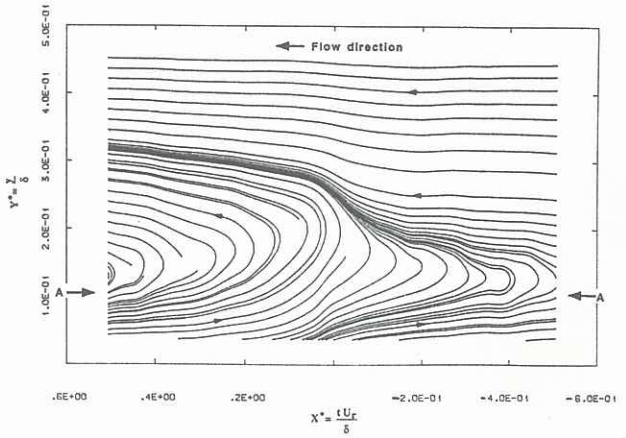

Figure 6 a. Conditionally averaged streamlines for strong Q2 events in the (x,y) plane.

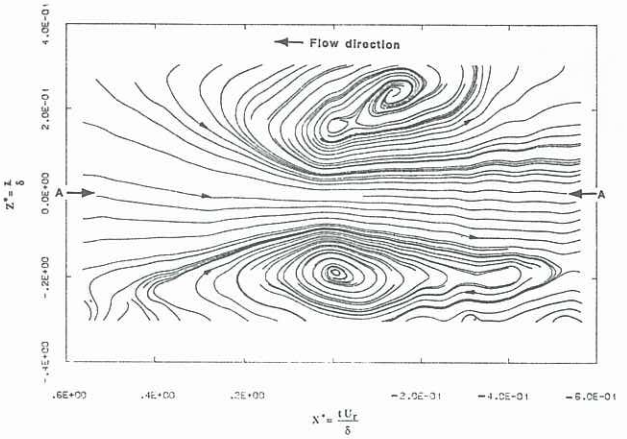

Figure 6 b. Conditionally averaged streamlines in the (x,z) plane based on detections of strong Q2 events in the (x,y) plane.

It may be argued that the symmetry observed in figure 6 (b) is an artifact of the conditional averaging. In most cases, the probe will not be at the center of the event. Since the probability that the center is in the upper or lower half of the array is the same, a symmetric pattern is expected. In order to try to locate the center of the events a scheme similar to the method used by Guezennec et al. (1989) in the (y,z) plane for DNS calculations of a channel flow was applied. The circulation, $\Gamma = \oint \mathbf{v} \cdot d\mathbf{r}$, close to the detection locations was computed for the three paths shown in figure 4 for each half of the rake data. The calculations were done on the measured data before interpolation and the sign and strength of the averages for each half was examined. Defining the complex quantity

$$G = \overline{\Gamma_{lower}} + i\overline{\Gamma_{upper}}$$

it was found that for weak Q2 events (H=0.844), the probability that the (x,z) plane flow pattern consists of two opposing large scale structures (quadrants 2 and 4 of G) was 57 % (based on 3492 detections). Most of these (77 %) were found in the second quadrant G_2. For each quadrant the normalized average asymmetry in circulation, defined as

$$\Delta\Gamma/\Gamma = \overline{\mid \Gamma_{upper} \mid - \mid \Gamma_{lower} \mid} / \overline{\mid \Gamma_{upper} \mid + \mid \Gamma_{lower} \mid}$$

was computed. This quantity, which was generally in the range -0.17 to 0.14, was 0.01 for G_2, showing that the most likely averaged pattern in fact consists of two opposing large scale structures of almost equal strength.

When the detection threshold was increased to H=4, the dominance of G_2 increased further with a probability of 62 % (based on 384 detections). Again the dominating G_2 events were almost symmetric with $\Delta\Gamma/\Gamma = 0.03$. Figure 7 (a) shows the conditional streamline patterns in this case. The probability of detecting structures rotating in the opposite direction (G_4) was, as expected, found to be small (6 %).

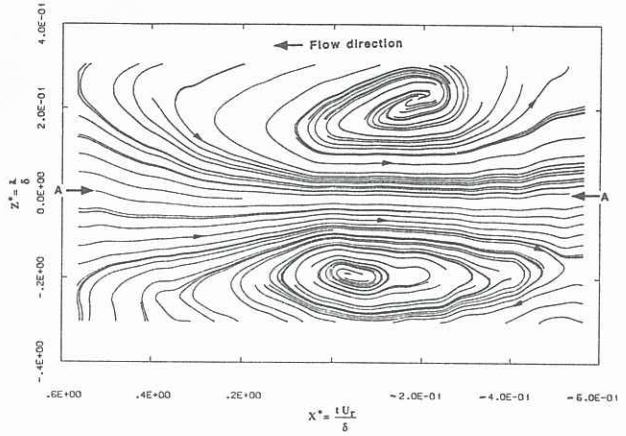

Figure 7 a. Conditionally averaged streamlines in the (x,z) plane based on the dominating counter-rotating structures.

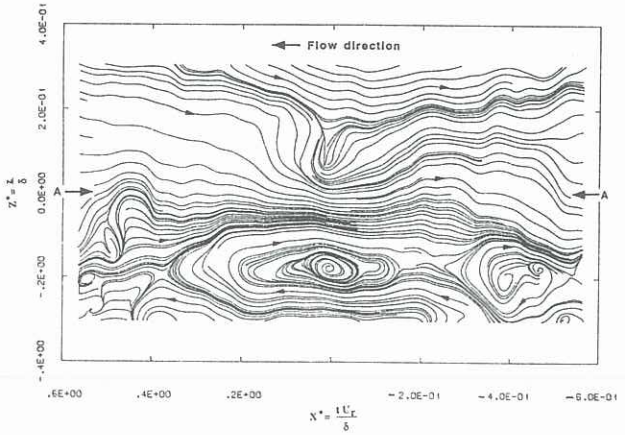

Figure 7 b. Conditionally averaged streamlines in the (x,z) plane based on co-rotating structures.

The probabilities for the co-rotating modes in quadrants 1 and 3 were found to be small and of about the same magnitude (12 and 20 % respectively) for strong Q2 events, but the asymmetry was much stronger ($\Delta\Gamma/\Gamma$ = -0.34 and $\Delta\Gamma/\Gamma = 0.31$ respectively) than for the counter-rotating detections. Therefore the detection of co-rotating flows is likely to occur when the probe intersects an event well away from its center. The streamline pattern for the G_3 detections is shown in figure 7 (b). (For co-rotating flows of opposite sign (G_1) a mirror image about the horizontal axis was obtained).

The previous statistics indicate that for strong Q2 events in the (x,y) plane the large scale symmetric pattern obtained from conditionally averaged data in the (x,z) plane is not an artifact of the averaging, but in fact the most probable flow pattern. It would clearly be of interest to infer the three-dimensional geometry of the large scale structures which give rise to strong Q2 events in the (x,y) plane.

CONCLUSIONS

An experimental method for obtaining velocities simultaneously from two orthogonal arrays of hot wires has been described. Although the method cannot yield complete information on three-dimensional aspects of the large scale motion, it provides some insight into the nature of this motion.

ACKNOWLEDGEMENT

The support of the Australian Research Council is gratefully acknowledged.

REFERENCES

Antonia, R. A. and Bisset, D. K. (1990) Three- dimensional aspects of the organized motion in a turbulent boundary layer, in M. Lesieur and O. Metais (eds.), Turbulence and coherent structures, Kluwer, 141-157

Bisset, D. K., Antonia, R. A. and Browne, L. W. B. (1990) Spatial organization of large structures in the turbulent far wake of a cylinder, J. Fluid Mech., **218**, 439-461

Guezennec, Y. G., Piomelli, U. and Kim, J. (1989) On the shape and dynamics of wall structures in turbulent channel flow, Phys. Fluids A, **1**, 764-766

Hussain, A. K. M. F. and Hayakawa, M. (1987) Eduction of large scale organized structures in a turbulent plane wake, J. Fluid Mech., **180**, 193-229

Kim, J. , Moin, P. and Moser, R. (1987) Turbulent statistics in fully developed channel flow at low Reynolds number, J. Fluid Mech., **177**, 133-166

Krogstad, P.-A. and Browne, L. W. B. (1991) Turbulent boundary layer flow over a rough surface, Report T.N. FM 91/1, Dept. of Mech. Eng., Univ. of Newcastle, Australia

Lu, S.S. and Wilmarth, W.W. (1973) Measurements of the Structure of the Reynolds Stress in a Turbulent Boundary Layer, J. Fluid Mech., **60**, 481-571

Nishino, K. and Kasagi, N. (1989) Turbulence statistics measurement in a two-dimensional channel flow using a three- dimensional particle tracking velocimeter, Proc. Seventh Symposium on Turbulent Shear Flows, Stanford University, 22.1.1-22.1.6

Spalart, P. R. (1988) Direct numerical simulation of a turbulent boundary layer up to $R_\theta = 1410$, J. Fluid Mech., **187**, 61-98